Journal of Organometallic Chemistry 882 (2019) 70–79

Contents lists available at ScienceDirect

Journal of Organometallic Chemistry

journal homepage: www.elsevier.com/locate/jorganchem

Synthesis of a heterometallic spiked tetrahedral cluster of ruthenium and nickel containing multiple hydrido ligands and its degradation to a tetrahedral $NiRu_3$ cluster

Takuya Kosukegawa, Toshiro Takao*

Department of Chemical Science and Engineering, School of Materials and Chemical Technology, Tokyo Institute of Technology, 2-12-1 O-okayama, Meguro-ku, Tokyo, 152-8552, Japan

ARTICLE INFO

Article history:
Received 6 December 2018
Received in revised form
25 December 2018
Accepted 26 December 2018
Available online 28 December 2018

Keywords:
Heterometallic cluster
Polyhydrido cluster
Spiked tetrahedron
Ni–Ru interaction
Fluxional behavior

ABSTRACT

A bimetallic spiked tetrahedral cluster of Ni and Ru, {Cp*Ru(H)(μ-H)$_3$}-{Ni(Cp*Ru)$_3$(μ$_3$-H)$_3$(μ-H)$_3$} (**2**) (Cp* = η^5-C$_5$Me$_5$), was synthesized by reaction of Cp*Ru(μ-H)$_4$RuCp* (**1**) with Ni(cod)2 under an atmosphere of H2. Cluster 2 comprises monomeric (Cp*RuH) and tetrahedral {Ni(Cp*Ru)$_3$(μ$_3$-H)$_3$(μ-H)$_3$} fragments linked by three bridging hydrogen atoms. Although site exchange of hydrides between the (Cp*RuH$_4$) and {Ni(Cp*Ru)$_3$H$_6$} moieties does not occur on the NMR time scale, incorporation of deuterium into the $NiRu_3$ fragment upon treatment of **2** with 1 atm of D_2 establishes that interfragment migration of hydrides does take place. Although reaction of **2** with ethylene results in the replacement of two hydrides in the spiked Ru center by an η^2-ethylene ligand, reaction with cyclopentadiene results in the degradation of the pentanuclear skeleton to a tetrahedral cluster, (CpNi)(Cp*Ru)$_3$(μ$_3$-H)$_3$(μ-H)$_3$ (**4**) (Cp = η^5-C$_5$H$_5$), and a mixed-ligand ruthenocene, Cp*CpRu (**5**).

1. Introduction

The synergistic effect arising from the presence of two different transition metals in close proximity to one another often yields dramatic improvements in catalytic activity and selectivity compared to the parent metals [1–5]. Nickel is a widely available transition element that exhibits high catalytic activity in dry reforming of methane [6] and hydrogen production from biomass [7–12]. However, its use is often problematic, because of a propensity for carbon deposition and sintering at high temperatures. To improve durability, addition of a noble metal to a Ni-based catalyst has been examined intensively [13]. Among bimetallic Ni-based catalysts, those of Ni and Ru have been widely employed and exhibit outstanding performance in the methanation of CO [14–18], steam and dry reforming of methane [19–24], conversion of biomass into valuable chemicals [25–28], hydrolytic dehydrogenation of ammonia borane [29–33], and hydrogenation of 3-hydroxypropanal to 1,3-propanediol [34].

Known structures of Ni–Ru bimetallic particles include a homogenous alloyed structure [22,24,35–41] and Ru@Ni [31,32,42,43] and Ni@Ru core–shell structures [18,29,30]. Although small particles of Ni and Ru can be dispersed separately on mesoporous alumina [15], TiO_2 [16], HZSM-5 [27], and N-doped active carbon [28], the reducibility of Ni particles is significantly enhanced by the presence of neighboring Ru particles. The role of Ru is proposed to be the catalytic reduction of neighboring Ni^{2+} via hydrogen spillover. This fact suggests that the mobility of hydride at the Ni–Ru site is crucial for the enhanced reactivity of bimetallic Ni/Ru catalysts.

Since the synthesis of the first heterometallic Ni/Ru cluster, Ru_3(CpNi)(μ-H)(μ$_4$-η^2-C=C^{t}BuH)(CO)$_9$ (Cp = η^5-C$_5$H$_5$), by Sappa and co-workers [44], many Ni/Ru complexes of various nuclearities (Ni_2Ru [45,46], $NiRu_2$ [47], $NiRu_3$ [44–46,48–53], Ni_2Ru_2 [54], $NiRu_4$ [55–57], Ni_2Ru_3 [46,58], $NiRu_5$ [59,60], and Ni_3Ru_3 [61]) have been prepared from $Ru_3(CO)_{12}$ and its derivatives. These heterometallic clusters are ideal precursors in the preparation of bimetallic Ni/Ru catalysts of well-defined composition. In addition, the nature of the anisotropic Ni–Ru bond in the clusters and the properties of hydrides at the Ni–Ru edge can provide important information concerning the distinctive reactivity of Ni/Ru catalysts. However, examples displaying a Ni–H–Ru interaction remain limited [53].

Wolf and co-workers synthesized a paramagnetic Ru_2Ni complex, which includes Ni–H–Ru interaction with a linear Ru^{II}–Ni^{II}–Ru^{II} arrangement, (PR$_3$)$_3$Ru(μ-H)$_3$Ni(μ-H)$_3$Ru(PR$_3$)$_3$ (R = C$_6$H$_4$-4-Me), by reaction of [RuH$_3$(PR$_3$)$_3$]$^-$ with Ni(acac)$_2$ [62]. The hydrido ligands were found by X-ray diffraction (XRD) to be

* Corresponding author.
E-mail address: takao.t.aa@m.titech.ac.jp (T. Takao).

https://doi.org/10.1016/j.jorganchem.2018.12.016
0022-328X/

much closer to the Ru atoms. The diminished covalent character of the Ni–H bonds has been supported by density functional theory (DFT) calculations, which produced estimated Wiberg bond index (WBI) values for the Ru–H and Ni–H bonds of 0.55 and 0.09, respectively.

The Ni–H–Ru interaction also is relevant to the core structure of [NiFe] hydrogenase. Ogo and co-workers demonstrated that [(NiL)Ru(H_2O)(η^6-C_6Me_6)]$^{2+}$ (L = *N,N′*-dimethyl-*N,N″*-bis(2-mercaptoethyl)-1,3-propanediamine) reacts with H_2 at ambient temperature to yield a monocationic μ-hydrido complex, [(NiL)(H_2O)(μ-H)Ru(η^6-C_6Me_6)]$^+$, via heterolytic H_2 cleavage [63]. Neutron diffraction revealed the bridging hydrido ligand to lie closer to the Ru atom, which suggests a noncovalent interaction between Ni and the hydride. A similar structural feature was reported by Rauchfuss and co-workers in [(*p*-cymene)Ru(μ-H)(μ-pdt)Ni(dppe)]$^+$ (pdt = 1,3-propanedithiolate) [64].

We previously reported synthesis of the heterometallic Ru/Pt cluster, {Cp*Ru(H_2)}$_2$Pt(μ-P^{t}Bu$_2$)$_2$(μ-H)$_2$ (Cp* = η^5-C_5Me_5), by reaction of Cp*Ru(μ-H)$_4$RuCp* (**1**) with Pt(P^{t}Bu$_3$)$_2$ [65]. The unsaturated nature of **1** effectively drives formation of a heterometallic architecture and provides multiple hydrides on the resulting heterometallic skeleton. Nakajima et al. examined the photochemical reaction of **1** with {CpNi(CO)}$_2$ (Cp = η^5-C_5H_5), which provided a tetrahedral cluster, (Cp*Ru)$_2$(CpNi)$_2$(μ$_3$-CO)$_2$ [66], albeit without a hydrido ligand. The absence of hydrides likely derives from the presence of CO, which can expel hydrides from the ruthenium centers. As an extension of our heterometallic polyhydrido cluster chemistry, we examined the reaction of **1** with non-carbonyl Ni species to construct a novel Ni/Ru skeleton with multiple hydrido ligands. In this article, we report the synthesis of a spiked tetrahedral Ru–$NiRu_3$ cluster containing multiple hydrides by reaction of **1** with Ni(cod)$_2$ (cod = 1,5-cyclooctadiene) and its degradation to a tetrahedral $NiRu_3$ cluster upon treatment with cyclopentadiene.

2. Results and discussion

2.1. Preparation of a pentanuclear Ru–$NiRu_3$ cluster

A novel diamagnetic pentanuclear $NiRu_4$ cluster, Cp*Ru(H)(μ-H)$_3$–Ni{Cp*Ru(μ$_3$-H)(μ-H)}$_3$ (**2**), was obtained by reaction of Cp*Ru(μ-H)$_4$RuCp* (**1**) with 0.5 equiv Ni(cod)$_2$ under 1 atm of H_2 (Eq. (1)). When the reaction was conducted under Ar, a mixture of several unidentified compounds was obtained. Thus, uptake of one molecule of dihydrogen appears to be essential for construction of the $NiRu_4$ skeleton.

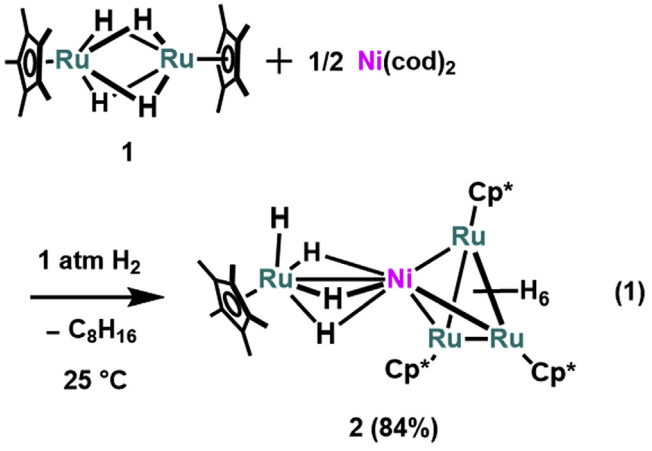

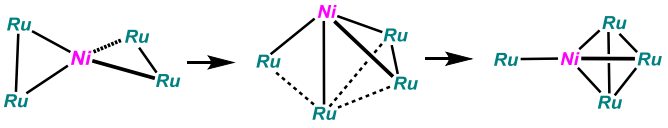

Scheme 1. Proposed formation mechanism of the spiked tetrahedral Ru–$NiRu_3$ core of **2**.

Although the formation mechanism of **2** is unclear at present, the fact that neither (Cp*Ru)$_3$(H)$_5$ [67] nor (Cp*Ru)$_4$(H)$_6$ [68] is produced suggests that the Ru–$NiRu_3$ spiked tetrahedron is formed by assembly of two molecules of dinuclear Ru^{III}–Ru^{III} and one molecule of a Ni^{II} species, likely [NiH_2], formed in situ (Scheme 1). The $NiRu_4$ species, which presumably adopts a bow tie skeleton centered on the nickel ion, then rearranges to the Ru–$NiRu_3$ spiked tetrahedron via an edge-bridged tetrahedral intermediate. Adams and Zhang showed that a bimetallic edge-bridged tetrahedron of iridium and ruthenium undergoes skeletal rearrangement to a Ru–$IrRu_3$ spiked tetrahedron upon treatment with CO [69]. Raithby and co-workers synthesized a spiked tetrahedral Ru–Os_4 cluster upon addition of P(OMe)$_3$ to the trigonal bipyramidal Os_4Ru cluster, which was obtained by reaction of [$Os_4(H)_2(CO)_{12}$]$^{2-}$ with [(η^6-C_6H_6)Ru(MeCN)$_3$]$^+$ [70].

The spiked tetrahedral Ru–$NiRu_3$ skeleton of **2** is unambiguously confirmed by XRD as shown in Fig. 1. The positions of the ten hydrido ligands were successfully established by Fourier synthesis. The metal core of **2** comprises a $NiRu_3$ tetrahedron with the Ni atom bonded to the [Cp*RuH] fragment through three bridging hydrides. The hydride in the [Cp*RuH] unit is coordinated to the Ru(4) atom in a terminal fashion. The remaining six hydrides are located with the $NiRu_3$ tetrahedron as μ- and μ$_3$-hydrides at each Ru–Ru edge and $NiRu_2$ face, respectively. The positions of hydrides in **2** are supported by DFT calculations as shown in Fig. 2.

Clusters adopting a spiked tetrahedral arrangement of five metal atoms are known [71–73]. Although all reported spiked tetrahedral

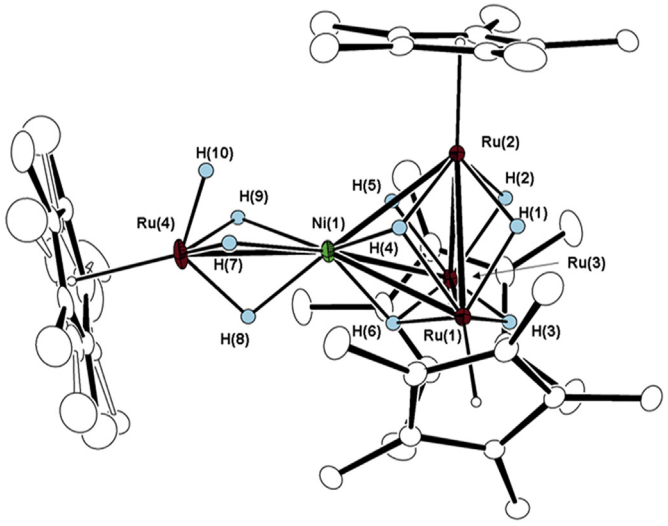

Fig. 1. Molecular structure and labeling scheme of **2** with thermal ellipsoids at 30% probability. Solvent molecule (1,4-dioxane) and hydrogen atoms in the Cp* groups were omitted for clarity. Selected bond lengths (Å) and angles (deg): Ni(1)–Ru(1) 2.6744(4), Ni(1)–Ru(2) 2.6777(4), Ni(1)–Ru(3) 2.6690(4), Ni(1)–Ru(4) 2.4490(4), Ru(1)–Ru(2) 2.7921(3), Ru(1)–Ru(3) 2.7918(3), Ru(2)–Ru(3) 2.7896(3), Ru(1)–Ni(1)–Ru(2) 62.891(10), Ru(1)–Ni(1)–Ru(3) 62.998(10), Ru(1)–Ni(1)–Ru(4) 141.969(15), Ru(2)–Ni(1)–Ru(3) 62.896(11), Ru(2)–Ni(1)–Ru(4) 142.966(16), Ru(3)–Ni(1)–Ru(4) 143.851(15), Ni(1)–Ru(1)–Ru(2) 58.613(10), Ni(1)–Ru(1)–Ru(3) 58.408(9), Ru(2)–Ru(1)–Ru(3) 59.943(9), Ni(1)–Ru(2)–Ru(1) 58.496(9), Ni(1)–Ru(2)–Ru(3) 58.400(9), Ru(1)–Ru(2)–Ru(3) 60.024(8), Ni(1)–Ru(3)–Ru(1) 58.594(9), Ni(1)–Ru(3)–Ru(2) 58.704(10), Ru(1)–Ru(3)–Ru(2), 60.034(8).

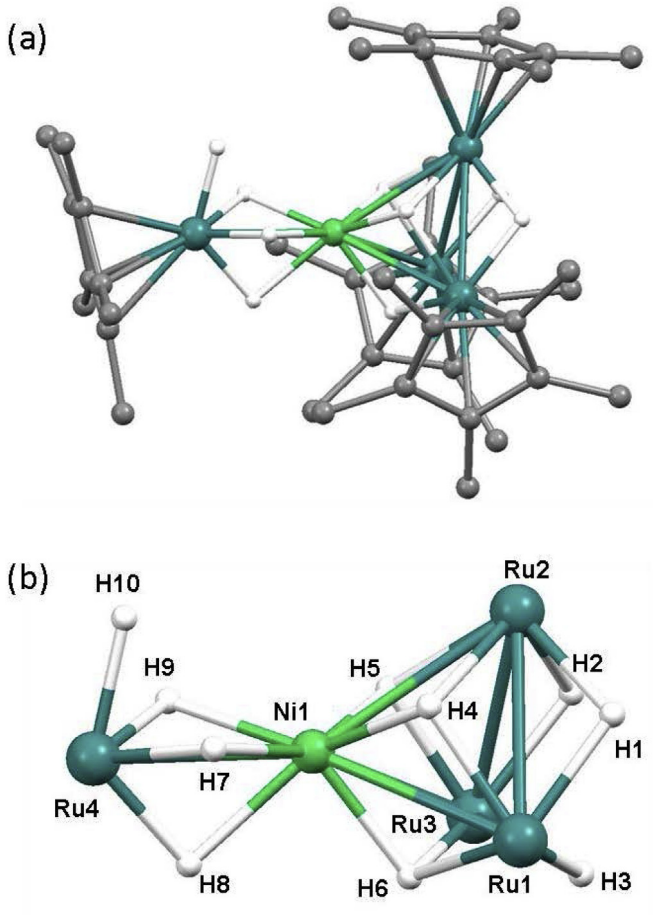

Fig. 2. (a) Optimized structure of **2** obtained by DFT calculations (ωB97XD/SDD (Ru, Ni), 6-31G(d) (C, H of Cp*), 6-311G(d,p) (H1–H10)), (b) Enlarged core view of **2**. Selected bond distances (Å): Ni1–Ru1 2.626, Ni1–Ru2 2.727, Ni1–Ru3 2.650, Ni1–Ru4 2.438, Ni1–H4 1.658, Ni1–H5 1.641, Ni1–H6 1.761, Ni1–H7 1.834, Ni1–H8 1.831, Ni1–H9 1.867, Ru1–Ru2 2.780, Ru1–Ru3 2.810, Ru1–H4 1.771, Ru1–H6 1.803, Ru2–Ru3 2.770, Ru2–H4 1.884, Ru2–H5 1.891, Ru3–H5 1.783, Ru3–H6 1.803, Ru4–H7 1.663, Ru4–H8 1.633, Ru4–H9 1.648, Ru4–H10 1.594.

clusters contain 76 valence electrons, the sum of the valence electrons of **2** is 72. Thus, **2** is electron deficient by four electrons relative to an electron precise configuration.

As mentioned below, the structural parameters of the $NiRu_3$ moiety in **2** are similar to those of isostructural $(CpNi)(Cp^*Ru)_3(\mu_3\text{-}H)_3(\mu\text{-}H)_3$ (**4**), which adopts a saturated tetrahedral structure containing 60 valence electrons. Assuming that the 18-electron $[Cp^*RuH_4]^-$ fragment in **2** serves as an ancillary ligand of the 54-electron $[Ni(Cp^*Ru)_3(\mu_3\text{-}H)_3(\mu\text{-}H)_3]^+$ unit, it should behave in a manner similar to an anionic six electron donor ligand such as Cp^-. Structure **A**, in which six electrons are supplied by σ-coordination of three Ru–H bonds to the Ni center, can be formally represented as one of the three resonance forms in Scheme 2.

In structure **A**, there is no bonding interaction between Ni(1) and Ru(4) despite the unusually short interatomic distance of 2.4489(4) Å. The Ni(1)–Ru(4) distance is considerably shorter than the unbridged Ni–Ru bond length in $Tp^{\#}Ni\text{–}RuCp(CO)_2$ (2.512(1) Å) ($Tp^{\#}$ = hydrotris(4-bromo-3,5-dimethylpyrazolyl)borato), which exhibits a 32-electron configuration [74]. A plausible explanation for the short distance is that the two metal nuclei are tightly linked by the three bridging hydrides. Wolf and co-workers detected no direct electronic interaction between the Ru and Ni atoms in $(PR_3)_3Ru(\mu\text{-}H)_3Ni(\mu\text{-}H)_3Ru(PR_3)_3$ (R = C_6H_4-4-Me) based on DFT calculations, although the interatomic distance is extremely short

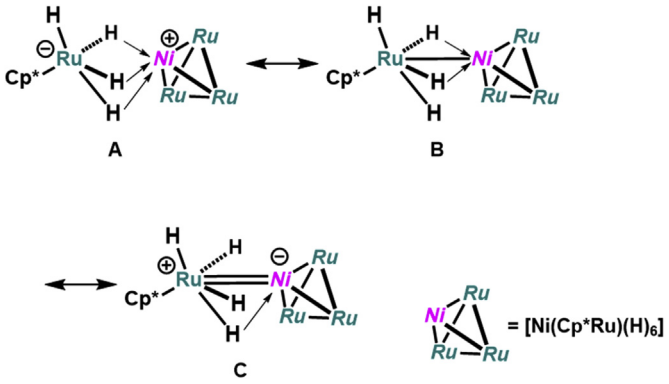

Scheme 2. Schematic explanation of the interaction between the $[Cp^*RuH_4]$ and $[Ni(Cp^*Ru)_3(H)_6]$ fragments in **2**.

(2.42172(18) Å) [62].

The Ru–H distances of the bridging hydrides at the Ru(4)–Ni(1) vertex (Ru(4)–H(7) 1.61(5) Å, Ru(4)–H(8) 1.58(4) Å, Ru(4)–H(9) 1.57(5) Å) are significantly shorter than the Ni–H distances (Ni(1)–H(7) 2.15(5) Å, Ni(1)–H(8) 1.76(4) Å, Ni(1)–H(9) 1.95(5) Å). XRD analysis does not provide intrinsically accurate structural data regarding hydrogen atoms bonded to a transition metal. However, the hydrogen atoms involved in the Ni–H–Ru interaction lie much closer to the Ru atom despite the larger covalent radius of Ru relative to that of Ni (Ru, 1.25 Å; Ni 1.10 Å).

The unsymmetrical coordination of the μ-hydrides at the spiked Ni–Ru vertex is reproduced in the optimized structure by DFT calculation: Ru4–H7 1.663 Å/Ni1–H7 1.834 Å, Ru4–H8 1.633/Ni1–H8 1.831, Ru4–H9 1.648 Å/Ni1–H9 1.867 Å. Natural orbital bond (NBO) analysis shows that the WBI value of the Ru–H bond (average 0.61) is much greater than that of the Ni–H bond (average 0.14) and is comparable to the value of the terminal Ru–H bond (0.66). These results are consistent with resonance form **A** in Scheme 2 and are similar to the structural features of previously reported Ni–H–Ru interactions [62–64].

The Ni(1) atom in the $NiRu_3$ tetrahedron lies nearly above the center of the Ru_3 plane defined by Ru(1), Ru(2), and Ru(3). The three Ni–Ru bonds in the $NiRu_3$ unit are almost identical in length: Ni(1)–Ru(1) 2.6744(4) Å, Ni(1)–Ru(2) 2.6777(4) Å, Ni(1)–Ru(3) 2.6690(4) Å. These values are greater than the unbridged Ni–Ru distances in $(CpNi)Ru_3(\mu\text{-}H)_3(CO)_7\{PPh_2CH_2CH_2Si(OEt)_3\}_2$ (average 2.560 Å), although the Ru–Ru distances in **2** (average 2.791 Å) are slightly shorter than the hydrido-bridged Ru–Ru distances in the same $NiRu_3$ cluster (average 2.879 Å) [75]. The Ni–Ru bond in the tetrahedral $NiRu_3$ moiety of **2** is lengthened likely owing to the presence of a μ_3-hydride, whereas the doubly bridged Ru–Ru bonds are shortened compared to the singly bridged Ru–Ru bond in $(CpNi)Ru_3(\mu\text{-}H)_3(CO)_7\{PPh_2CH_2CH_2Si(OEt)_3\}_2$.

Brivio and co-workers reported the XRD structure of an anionic $NiRu_3$ cluster, $[NiRu_3(\mu_3\text{-}H)(CO)_9(\mu\text{-}CO)_3]^-$, which is the only example of a structurally determined μ_3-hydride on a $NiRu_2$ face [53]. The Ni–(μ_3-H) distance in the Brivio's complex (1.85(7) Å) is slightly greater than the Ru–(μ_3-H) lengths (1.73(6), 1.80(6) Å). In contrast, the Ni–(μ_3-H) distance in **2** (average 1.69(4) Å) is shorter than the average Ru–(μ_3-H) distance (1.80(4) Å). The 0.11 Å difference is consistent with the difference in the covalent radii. This feature is reproduced by DFT calculations, which yield WBI values of 0.28 for Ru–(μ_3-H) and 0.19 for Ni–(μ_3-H). Thus, the μ_3-hydrides on the $NiRu_2$ face appear to be coordinated to the three metal centers in an almost symmetrically manner, unlike the μ-hydrides at the spiked Ni–Ru vertex.

The ^1H NMR spectrum of **2** recorded at −80 °C displays Cp*

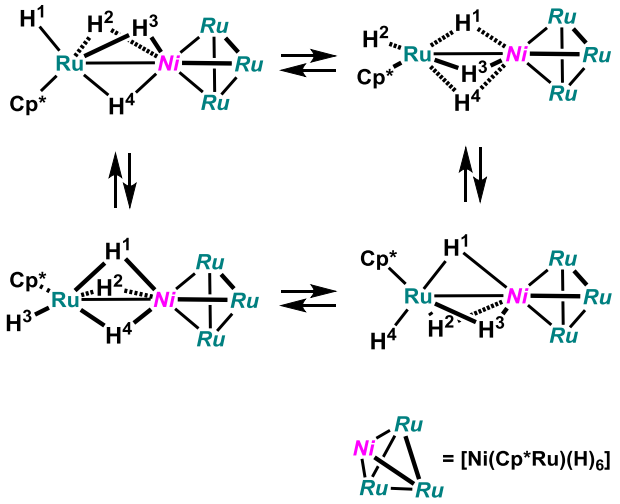

Scheme 3. Rapid rotation of [Cp*RuH$_4$] around the Ni–Ru axis.

signals at δ 2.11 and 1.79 ppm with an intensity ratio of 3:1. This indicates that the spiked (Cp*RuH$_4$) moiety rotates rapidly within the NMR time scale, producing a time averaged C_3 structure. The four hydrides attached to Ru(4), which resonate at δ −14.19, are also equivalent at −80 °C. This result indicates that the rotation of the (Cp*RuH$_4$) moiety proceeds via the interconversion of hydrides between terminal and bridging positions as shown in Scheme 3.

Two singlets derived from the hydride ligands in the NiRu$_3$ unit are observed at δ −12.41 and −16.06 ppm at −40 °C with equal intensities. The signals broaden with increasing temperature and become buried beneath the base line at 40 °C (Fig. 3). This spectral behavior is caused by site exchange of hydrides between the μ$_3$-and μ-positions on the NiRu$_3$ tetrahedron. The activation parameters of this structural conversion are estimated by spectral simulation to be $\Delta H^{\ddagger} = 15.5 \pm 0.3$ kcal mol^{-1} and $\Delta S^{\ddagger} = 7.0 \pm 1.0$ cal mol^{-1} K^{-1}.

The shape of the (Cp*RuH$_4$) hydride signal does not change as a function of temperature. This indicates that site exchange of hydrides between (Cp*RuH$_4$) and {Ni(Cp*Ru)$_3$H$_6$} does not occur within the NMR time scale.

All hydrido ligands of **2** are deuterated when the cluster is treated with 1 atm of D$_2$ at 25 °C. However, the deuteration ratio at each position is different. Although 70% of the hydrides are deuterated in the spiked (Cp*RuH$_4$) moiety after 48 h, the deuteration ratio reaches only 15% in NiRu$_3$. The slow exchange on the NiRu$_3$ center suggests that deuterium atoms are incorporated exclusively into the spiked Ru center and migrate to the NiRu$_3$

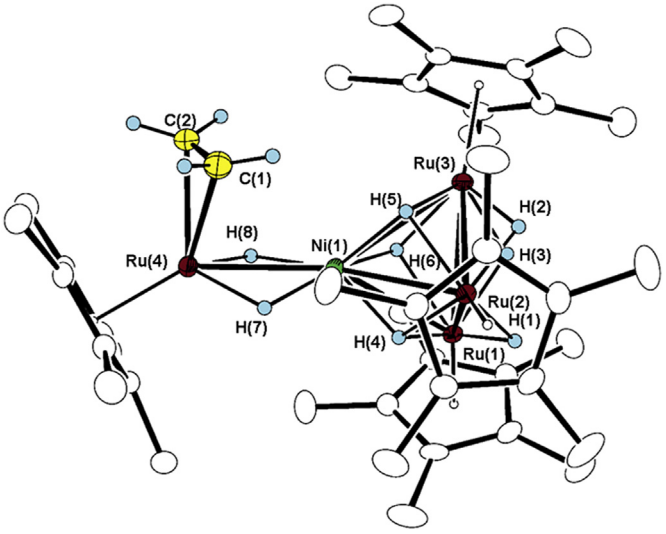

Fig. 4. Molecular structure and labeling scheme of **3** with thermal ellipsoids at 30% probability. A solvent molecule (*n*-hexane) and hydrogen atoms of the Cp* groups are omitted for clarity. Selected bond lengths (Å) and angles (deg): Ni(1)–Ru(1) 2.6798(3), Ni(1)–Ru(2) 2.6580(3), Ni(1)–Ru(3) 2.7351(3), Ni(1)–Ru(4) 2.5412(3), Ru(1)–Ru(2) 2.8009(3), Ru(1)–Ru(3) 2.7607(3), Ru(2)–Ru(3) 2.7886(3), Ru(4)–C(1) 2.163(3), Ru(4)–C(2) 2.158(3), C(1)–C(2) 1.391(5), Ru(1)–Ni(1)–Ru(2) 63.297(8), Ru(1)–Ni(1)–Ru(3) 61.295(9), Ru(1)–Ni(1)–Ru(4) 147.365(13), Ru(2)–Ni(1)–Ru(3) 62.252(9), Ru(2)–Ni(1)–Ru(4) 136.479(14), Ru(3)–Ni(1)–Ru(4) 145.514(13), Ni(1)–Ru(1)–Ru(2) 57.971(8), Ni(1)–Ru(1)–Ru(3) 60.339(8), Ru(2)–Ru(1)–Ru(3) 60.181(7), Ni(1)–Ru(2)–Ru(1) 58.732(8), Ni(1)–Ru(2)–Ru(3) 60.229(8), Ru(1)–Ru(2)–Ru(3) 59.195(7), Ni(1)–Ru(3)–Ru(1) 58.366(8), Ni(1)–Ru(3)–Ru(2) 57.518(8), Ru(1)–Ru(3)–Ru(2), 60.624(7).

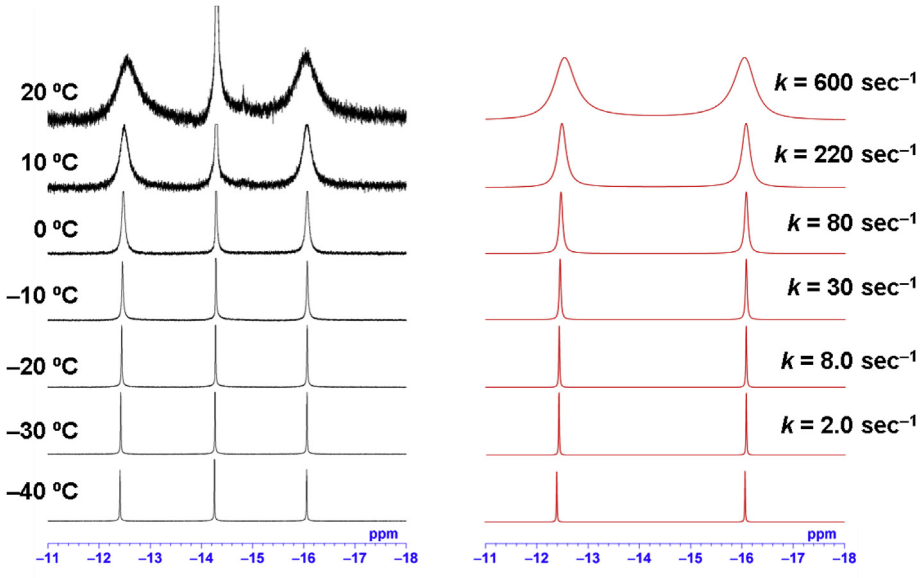

Fig. 3. (left) Variable temperature ^{1}H NMR spectra of the hydride region of **2** (400 MHz, THF-d_6). (right) Simulated spectra represent the site exchange between μ$_3$-and μ-hydrides on the NiRu$_3$ moiety.

moiety. Variable temperature NMR experiments establish the rate of the hydride migration between (Cp^*RuH_4) and ($NiRu_3H_6$) to be much less than the NMR time scale. Although a path involving direct reaction of D_2 at $NiRu_3$ is not excluded, the fact that $(Cp^*Ni)(Cp^*Ru)_3(\mu_3\text{-}H)_3(\mu\text{-}H)_3$ (**4**) does not react with D_2 at 25 °C strongly suggests that hydride migration from the spiked Ru center to the $NiRu_3$ moiety is slow.

The proposal that the spiked Ru atom acts as a reaction site in **2** is supported by the reaction of **2** with ethylene, which yields $\{Cp^*Ru(\mu\text{-}H)_2(C_2H_4)\}$–$\{Ni(Cp^*Ru)_3(\mu_3\text{-}H)_3(\mu\text{-}H)_3\}$ (**3**) that contains an η^2-ethylene ligand at the spiked Ru atom (Eq. (2)). Complex **2** reacts with 1 atm of ethylene at 25 °C in 48 h with elimination of two hydrides as ethane, as confirmed by a singlet at δ 0.80 ppm. Treatment of **3** with 1 atm of H_2 at 25 °C regenerates **2** with eliminating ethane, although the reaction is extremely slow (5% in 24 h).

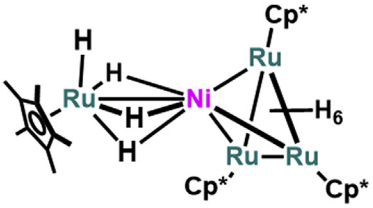

2

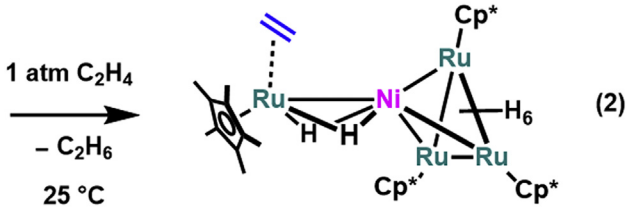

(2)

3 (78%)

The XRD structure of **3** demonstrates that the ethylene molecule is coordinated to Ru(4) in an η^2 fashion (Fig. 4). The C(1)–C(2) bond length (1.391(5) Å) is similar to that in $\{Cp^*Ru(C_2H_4)\}_2Pt(\mu\text{-}P^tBu_2)_2(\mu\text{-}H)_2$ (1.398(5) Å) [65]. The number of hydrides bridging Ni(1) and Ru(4) decreases from three to two upon incorporation of ethylene, which slightly increases the Ni(1)–Ru(4) distance from 2.4490(4) Å in **2** to 2.5412(3) Å. Unsymmetrical coordination of H(7) and H(8) at the Ni(1)–Ru(4) site is still observed in **3** (Ru(4)–H(7) 1.59(3) Å/Ni(1)–H(7) 1.70(3) Å, Ru(4)–H(8) 1.67(3) Å/Ni(1)–H(8) 1.74(3) Å). Other structural parameters, primarily within the $NiRu_3$ unit, are similar to those of **2**.

The ^{1}H NMR spectrum of **3** also contains Cp* signals at δ 2.11 and 1.76 ppm with an intensity ratio of 3:1, which indicates that **3** retains a pseudo C_3 structure in solution. This likely occurs by rotation of the $Cp^*Ru(C_2H_4)(H)_2$ unit around the Ni(1)–Ru(4) axis. The signals arising from the μ_3-and μ-hydrides in the $NiRu_3$ center are equivalent at 25 °C, indicating that site exchange of hydrides between the two positions occurs as in **2**.

2.2. Preparation of a tetrahedral $NiRu_3$ cluster

Reactions of **2** with dienes were examined to explore the influence of the neighboring Ni atom on transformations of the substrate coordinated to the spiked Ru atom. Only a mixture of unidentified products was obtained upon reaction with isoprene. However, reaction of **2** with cyclopentadiene proceeds cleanly to yield a tetrahedral cluster, $(CpNi)(Cp^*Ru)_3(\mu_3\text{-}H)_3(\mu\text{-}H)_3$ (**4**), accompanied by formation of a mixed ligand ruthenocene, Cp^*CpRu (**5**) (Eq. (3)).

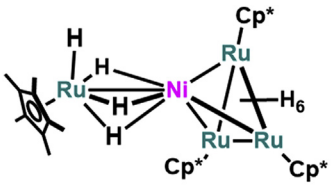

2

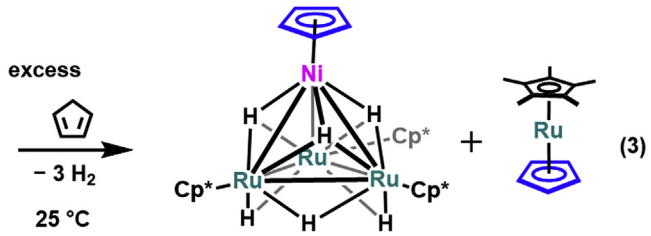

(3)

4 (91%) **5**

We previously observed that **5** is formed upon thermolysis of the diruthenium $\mu\text{-}\eta^2\text{:}\eta^2$-cyclopentadiene complex, $\{Cp^*Ru(\mu\text{-}H)\}_2(\mu\text{-}\eta^2\text{:}\eta^2\text{-}C_5H_6)$ [76]. Formation of **5** in Eq. (3) is fully consistent with $\mu\text{-}\eta^2\text{:}\eta^2$-coordination of cyclopentadiene at the spiked Ni–Ru vertex, whereas no intermediate containing a bridging hydrocarbyl ligand at the Ni–Ru edge is observed.

A single crystal for XRD analysis was obtained from a cold toluene solution of **4**. The structure of **4** is shown in Fig. 5a. The positions of six hydrides were successfully determined by Fourier synthesis as seen in the $NiRu_3$ moieties in **2** and **3**, that is, three μ-hydrides and three μ_3-hydrides. Their locations are also supported by DFT calculations illustrated in Fig. 5b.

As found in the $NiRu_3$ moiety of **2**, the three Ni–Ru lengths in **4** are nearly equal (2.6714(4)–2.6932(4) Å) and of comparable value to those of **2** (average 2.67 Å) and **3** (average 2.69 Å). The Ru–Ru distances range from 2.8086(3) to 2.8211(3) Å and also are similar to those of **2** (average 2.79 Å) and **3** (average 2.78 Å). The tendency that the Ni–(μ_3-H) bond lengths are shorter than the Ru–(μ_3-H) lengths is also observed in **4** (average Ni–(μ_3-H) 1.64 Å; average Ru–(μ_3-H) 1.87 Å).

The Ni–Ru and Ru–Ru distances are well reproduced in the optimized structure (average Ni–Ru, 2.678 Å; average Ru–Ru 2.826 Å). The Ni–(μ_3-H) and Ru–(μ_3-H) distances in the optimized structure are estimated to be 1.70 and 1.83 Å, respectively. The values are comparable to those optimized for **2** (Ni–H 1.69 Å, Ru–H 1.82 Å). The WBI values for these bonds are estimated to be 0.27 and 0.22, respectively, which suggests symmetrical coordination of the μ_3-hydrides at the $NiRu_2$ face.

Two sharp hydride signals are observed at δ −12.92 and −17.27 ppm in the ^{1}H NMR spectrum of **4** recorded at −70 °C. The resonances broaden with increasing temperature similar to the hydride signals in **2** (Fig. 6). The estimated activation parameters of the spectral change based on spectral simulations are $\Delta H^{\ddagger} = 14.6 \pm 0.2$ kcal mol^{-1} and $\Delta S^{\ddagger} = 9.8 \pm 1.0$ cal mol^{-1} K^{-1}. The values are comparable to those observed for **2** ($\Delta H^{\ddagger} = 15.5 \pm 0.3$ kcal mol^{-1}, $\Delta S^{\ddagger} = 7.0 \pm 1.0$ cal mol^{-1} K^{-1}).

The sum of the valence electrons in **4** (60-electron) is precisely the number expected for a tetrahedral cluster, which makes **4**

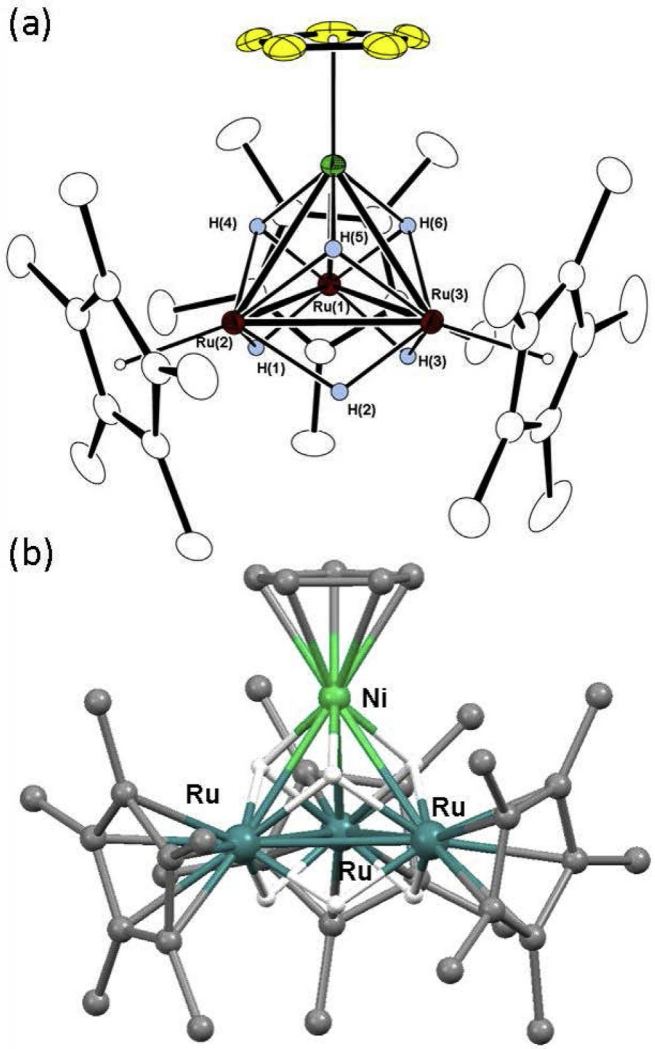

Fig. 5. (a) Molecular structure and labeling scheme of **4** with thermal ellipsoids at 30% probability. Selected bond lengths (Å) and angles (deg): Ni(1)–Ru(1) 2.6926(4), Ni(1)–Ru(2) 2.6932(4), Ni(1)–Ru(3) 2.6714(4), Ru(1)–Ru(2) 2.8086(3), Ru(1)–Ru(3) 2.8176(3), Ru(2)–Ru(3) 2.8211(3), Ru(1)–Ni(1)–Ru(2) 62.864(9) Ru(1)–Ni(1)–Ru(3) 63.372(9), Ru(2)–Ni(1)–Ru(3) 63.452(9), Ni(1)–Ru(1)–Ru(2) 58.578(9), Ni(1)–Ru(1)–Ru(3) 57.947(8), Ru(2)–Ru(1)–Ru(3) 60.188(7), Ni(1)–Ru(2)–Ru(1) 58.558(9), Ni(1)–Ru(2)–Ru(3) 57.898(8), Ru(1)–Ru(2)–Ru(3) 60.063(7), Ni(1)–Ru(3)–Ru(1) 58.681(9), Ni(1)–Ru(3)–Ru(2) 58.650(9), Ru(1)–Ru(3)–Ru(2), 59.748(7), (b) Optimized structure of **4** obtained by DFT calculations (B3PW91/SDD (Ru, Ni), 6-31G(d) (C, H of Cp* and Cp), 6-311G(d,p) (H1–H6)). Selected bond lengths (Å): Ni1–Ru1 2.677, Ni1–Ru2 2.684, Ni1–Ru3 2.674, Ru1–Ru2 2.824, Ru1–Ru3 2.828, Ru2–Ru3 2.826.

thermally stable. Complex **4** does not decompose upon heating at 80 °C for at least 24 h and, unlike **2**, does not exhibit H/D exchange under 1 atm D_2. These results indicate that reductive elimination of hydrides from **4**, which would produce a vacant site at the $NiRu_3$ center, does not occur readily. Partial rupture of the tetrahedral skeleton leading to formation of a butterfly structure, which is another means of generating a vacant site, may be prevented by strong bonding of the μ_3-hydrides to the three metal nuclei.

Lavigne and co-workers synthesized a closely related 60-electron $NiRu_3$ cluster, $(CpNi)Ru_3(CO)_9(\mu\text{-}H)_3$, by reaction of $Ru_3(CO)_{12}$ with $\{CpNi(\mu\text{-}CO)\}_2$ under 1 atm of H_2 [51]. Sappa and co-workers showed that $(CpNi)Ru_3(CO)_9(\mu\text{-}H)_3$, unlike **4**, undergoes deuteration upon heating under a D_2 atmosphere despite its saturated configuration [77]. They also observed $(CpNi)Ru_3(CO)_9(\mu\text{-}H)_3$ to fragment readily upon heating in a N_2 atmosphere. These results suggest that H/D exchange in $(CpNi)Ru_3(CO)_9(\mu\text{-}H)_3$ occurs via partial breaking of the tetrahedral skeleton, most likely by cleavage of an unsupported Ni–Ru bond.

In contrast, the Ni–Ru bonds in **4** are supported by μ_3-hydrido ligands. Although the μ_3-hydrides suppress degradation of the cluster skeleton, they make it difficult to generate a vacant site via Ni–Ru bond cleavage. Therefore, it is anticipated that reactivity will be improved by removing a μ_3-hydride from the $NiRu_3$ frame. Protonation of a hydrido complex followed by reductive elimination of dihydrogen is often employed to generate a coordinatively unsaturated species. Protonation of **4** was thus examined, but the reaction resulted in degradation of the $NiRu_3$ skeleton and produced a cationic triruthenium complex, $[Cp^*Ru(\mu\text{-}H)_2]_3^+$ [67].

3. Conclusion

In summary, a novel bimetallic spiked tetrahedral cluster of Ni and Ru, $\{Cp^*Ru(H)(\mu\text{-}H)_3\}$–$\{Ni(Cp^*Ru)_3(\mu_3\text{-}H)_3(\mu\text{-}H)_3\}$ (**2**), was synthesized by reaction of $Cp^*Ru(\mu\text{-}H)_4RuCp^*$ (**1**) with $Ni(cod)_2$ under a H_2 atmosphere. The structural parameters of the tetrahedral fragment in **2** are very similar to those of the 60-electron $NiRu_3$ tetrahedron, $(CpNi)(Cp^*Ru)_3(\mu_3\text{-}H)_3(\mu\text{-}H)_3$ (**4**). This property suggests that the spiked $[Cp^*RuH_4]^-$ fragment acts as a six-electron donor to the $NiRu_3$ unit. $[Cp^*RuH_4]^-$ can provide six-electrons to the Ni center through σ-coordination of the Ru–H bonds. Unsymmetrical coordination of the μ-hydrides at the spiked Ni–Ru vertex in a manner similar to reported Ni–H–Ru interactions [62–64] is supported by DFT calculations.

The spiked Ru atom acts as a site for reaction with D_2, ethylene, and, presumably, cyclopentadiene. Deuterium is incorporated into the $NiRu_3$ moiety of **2** although the tetrahedral $NiRu_3$ complex **4** does not react with D_2. Although the rate of the site exchange is slow on the NMR time scale, the migration of hydride between the (Cp^*RuH_4) and $\{Ni(Cp^*Ru)_3(H)_6\}$ fragments could be a model of a hydrogen atom spillover in bimetallic Ni/Ru catalysts.

Reaction of **2** with cyclopentadiene displaces the spiked (Cp^*RuH_4) fragment and form the tetrahedral $NiRu_3$ tetrahedral cluster, **4**, exclusively. Complex **4** resists H/D exchange with D_2, likely because of its precise 60-electron configuration and the presence of μ_3-hydrides on each $NiRu_2$ face. We are continuing to study the reactivity of **2** toward other unsaturated hydrocarbons and the synthesis of reactive $NiRu_3$ species derived from **4** by dihydrogen removal from the cluster core.

4. Experimental

4.1. General procedures

All compounds were manipulated using standard Schlenk and high-vacuum-line techniques under an atmosphere of argon. Dehydrated toluene, acetonitrile, and hexane used in this study were purchased from Kanto Chemicals and stored under an atmosphere of argon. 1,4-dioxane was dried over $LiAlH_4$ and stored under an argon atmosphere. Monomeric cyclopentadiene was obtained by the cracking of dicyclopentadiene. C_6D_6 and THF-d_8 were dried over sodium–benzophenone ketyl and stored under an atmosphere of argon. Dichloromethane-d_2 was dried over phosphorus pentoxide and stored under an argon atmosphere. $Ni(cod)_2$ was purchased from Aldrich and stored under an argon atmosphere. Other reagents were used as received. Diruthenium tetrahydrido complex, $Cp^*Ru(\mu\text{-}H)_4RuCp^*$ (**1**), was prepared according to the published method [78]. ^1H and ^{13}C NMR spectra were recorded on Varian INOVA-400 and Varian 400 MR spectrometers. ^1H NMR spectra were referenced to tetramethylsilane as an internal standard. ^{13}C NMR spectra were referenced to the natural-

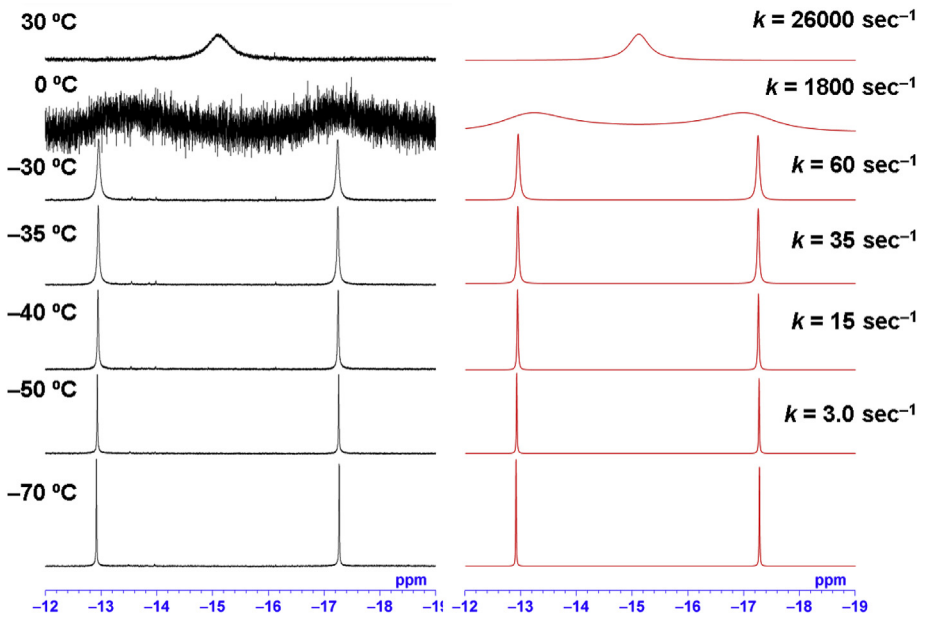

Fig. 6. (left) Variable temperature ^{1}H NMR spectra of **4** showing the hydride region (400 MHz, THF-d_8). (right) Simulated spectra.

abundance carbon signal of the solvent employed. Elemental analyses were performed on a PerkinElmer 2400II CHN analyzer.

4.2. Variable temperature NMR studies and simulations

Variable-temperature NMR studies were performed in NMR tubes equipped with a J. Young valve using a Varian INOVA-400 Fourier transform spectrometer. The NMR simulations for the temperature-dependent hydride signals of **2** and **4** were performed using gNMR v5.0.6.0 (2006, Ivory Soft) via an iterative parameter search upon the exchange constants, k, which was the rates for the site-exchange of hydrides between the μ_3-and μ-positions. The rate constants accurately modeled the experimental spectra at each temperature. The activation parameters $\Delta H^{\ddagger}$ and $\Delta S^{\ddagger}$ were determined from the plot of ln(k/T) versus 1/T. Estimated standard deviations (σ) in the slope and y intercept of the Eyring plot determined the error in $\Delta H^{\ddagger}$ and $\Delta S^{\ddagger}$, respectively. The standard deviation in $\Delta G^{\ddagger}$ was determined from the formula: $\sigma(\Delta G^{\ddagger})^2 = \sigma(\Delta H^{\ddagger})^2 + [\mathrm{T}\sigma(\Delta S^{\ddagger})]^2 - 2\mathrm{T}\sigma(\Delta H^{\ddagger})\,\sigma(\Delta S^{\ddagger})$.

4.3. X-ray diffraction studies

Single crystals of **2**, **3**, and **4** for the X-ray analyses were obtained directly from the preparations described below and mounted on nylon Cryoloops with Paratone-N (Hampton Research corp.). Diffraction experiment was performed on a Rigaku R-AXIS RAPID imaging plate diffractometer with graphite-monochromated Mo-Kα radiation ($\lambda = 0.71069$ Å). Cell refinement and data reduction were performed using the PROCESS-AUTO program [79]. Intensity data were corrected for Lorentz-polarization effects and for numerical and empirical absorption. The structures were solved by the direct method using SHELXT-2018/1 and further refined with the SHELXL-2016/6 program package [80,81]. All non-hydrogen atoms were found by a difference Fourier synthesis and were refined anisotropically. The refinement was carried out by least-squares methods based on F^2 with all measured reflections. For **2**, the Cp* group attached to the Ru(4) atom was disordered with 62%:38% occupancy. The cocrystallized 1,4−dioxane was disordered over two sites with 62%:38% occupancy. The enhanced rigid-bond restraint (SHELX keyword RIGU) was applied to the disordered Cp* group and the 1,4-dioxane molecule [82]. The metal-bound hydrogen atoms in **2**, **3** and **4** were found by the difference synthesis and refined isotropically. Hydrogen atoms in the 1,4-dioxane molecule cocrystallized with **2** could not be located. Crystal data and results of the analyses are listed in Table S1 in the Supplementary Material. The CIF data of **2**, **3**, and **4** are deposited in the Cambridge Crystallographic Data Center with the deposition numbers of 1886670 (**2**), 1886671 (**3**), and 1886672 (**4**).

4.4. Computational details

DFT calculations were carried out at the ωB97XD level for **2** and B3PW91 level for **4** in conjunction with the Stuttgart/Dresden ECP [83] and associated with triple-ζ SDD basis sets for Ru and Ni [84]. For H and C of the Cp* and Cp groups, 6-31G(d) basis sets were employed. For metal-bound hydrogen atoms, 6-311G(d,p) basis sets were employed. No simplified model compounds were used for the calculations. Initial geometries for the optimization were based on the crystallographically determined structure of **2** and **4**. Calculations were performed using the Gaussian 16 software suite [85]. The molecular structures were drawn using the GaussView version 6.0 program [86]. Frequency calculations at the same level of theory as geometry optimizations were performed on the optimized structure to ensure that minima exhibit only positive frequency. Information on the atom coordinates (xyz files) for all optimized structures are given in the Supplementary Material.

4.5. Preparations

4.5.1. {Cp*Ru(H)(μ-H)$_3$}−{Ni(Cp*Ru)$_3$(μ_3-H)$_3$(μ-H)$_3$} (**2**)

A 300 mL Schlenk tube was charged with **1** (0.418 g, 0.877 mmol), Ni(cod)$_2$ (0.123 g, 0.448 mmol). After the flask was cooled at −78 °C by a dry ice/methanol bath, toluene (50 mL) was added. After the flask was degassed at −78 °C, 0.1 MPa of dihydrogen was introduced. The solution was warmed to 25 °C by removing the flask from the cooling bath. The solution was vigorously stirred for 3 days at 25 °C. The color of the solution changed from dark-red to deep green. After concentrating the solution

under reduced pressure, the solution was passed through a short alumina pad to remove a Ni powder. The filtrate was then dried under reduced pressure. A 0.376 g amount of {Cp*Ru(H)(μ-H)$_3$}-{Ni(Cp*Ru)$_3$(μ$_3$-H)$_3$(μ-H)$_3$} (**2**) was obtained as a crystalline black solid (0.371 mmol, 85% based on **1**). A black single crystal including one molecule of 1,4-dioxane was obtained from the cold 1,4-dioxane solution of **2** stored at 0 °C. ^{1}H NMR (400 MHz, THF-d_8, −80 °C): δ −16.02 (s, 3H, μ- or μ$_3$-*H* in the NiRu$_3$ moiety), −14.19 (s, 4H, Ru*H*Ni and Ru*H* in the Cp*RuH$_4$ moiety), −12.35 (s, 3H, μ- or μ$_3$-*H* in the NiRu$_3$ moiety), 1.79 (s, 15H, C$_5$*Me*$_5$), 2.11 ppm (s, 45H, C$_5$*Me*$_5$). ^{13}C{^{1}H} NMR (100 MHz, THF-d_8, 25 °C): δ 12.7 (C$_5$*Me*$_5$ in the Cp*RuH$_4$ moiety), 13.3 (C$_5$*Me*$_5$ in the NiRu$_3$ moiety), 92.3 (*C*$_5$Me$_5$ in the NiRu$_3$ moiety), 93.3 ppm (*C*$_5$Me$_5$ in the Cp*RuH$_4$ moiety). Anal. Calcd for C$_{40}$H$_{70}$NiRu$_4$: C, 47.38; H, 6.96. Found: C, 47.37; H, 6.97.

*4.5.2. Reaction of **2** with 1 atm of D_2*

An NMR tube equipped with a Teflon valve was charged with **2** (5.0 mg, 4.9 μmol) and THF-d_8 (0.4 mL). After the NMR tube was degassed with a liquid N_2 bath, 1 atm of D_2 was introduced. The NMR tube was kept at 25 °C. The ^{1}H NMR spectrum recorded after 48 h showed the signals derived from isotopomers of **2**. The ratios of deuteration at each hydride signal were calculated based on the differences of the signal intensities from those recorded before introduction of D_2 and estimated at 18%, 71%, and 11% for the signals at δ −12.41, −14.26, −16.06 ppm.

*4.5.3. {Cp*Ru(μ-H)$_2$(η^2-C$_2$H$_4$)}−{Ni(Cp*Ru)$_3$(μ$_3$-H)$_3$(μ-H)$_3$} (**3**)*

A 50 mL Schlenk tube was charged with **2** (48.8 mg, 48.1 μmol) and toluene (5.0 mL). After the flask was degassed by the freeze-pump-thaw cycle two times, 0.1 MPa of ethylene was introduced at 25 °C. The solution was vigorously stirred for 2 days at 25 °C. The color of the solution changed from deep green to dark green. After the solvent was removed under reduced pressure, the resulting solid was extracted with 10 mL of hexane. The solution was then concentrated to *ca.* 5 mL under reduced pressure and stored at −30 °C. Drying the precipitate under reduced pressure afforded 38.5 mg amount of **3** as a black chunk (37.0 μmol, 77%). A black single crystal including one molecule of hexane was obtained from the cold hexane solution of **3** stored at −30 °C. ^{1}H NMR (400 MHz, C$_6$D$_6$, 25 °C): δ −16.09 (s, 2H, Ru*H*Ni in the Cp*Ru(C$_2$H$_4$)H$_2$ moiety), −14.68 (br, 6H, μ- and μ$_3$-*H* in the NiRu$_3$ moiety), 1.76 (s, 15H, C$_5$*Me*$_5$), 2.11 (s, 45H, C$_5$*Me*$_5$), 2.23 ppm (br, 4H, C$_2$*H*$_4$). ^{13}C NMR (100 MHz, C$_6$D$_6$, 25 °C): δ 11.0 (q, J_{CH} = 125 Hz, C$_5$*Me*$_5$ in the Cp*RuH$_4$ moiety), 13.0 (q, J_{CH} = 127 Hz, C$_5$*Me*$_5$ in the NiRu$_3$ moiety), 24.8 (t, J_{CH} = 154 Hz, *C*$_2$H$_4$), 88.8 (*C*$_5$Me$_5$ in the Cp*RuH$_4$ moiety), 91.9 ppm (*C*$_5$Me$_5$ in the NiRu$_3$ moiety). Anal. Calcd for C$_{42}$H$_{72}$NiRu$_4$: C, 48.51; H, 6.98. Found: C, 48.34; H, 7.38.

*4.5.4. (CpNi)(Cp*Ru)$_3$(μ$_3$-H)$_3$(μ-H)$_3$ (**4**)*

A 50 mL Schlenk tube was charged with **2** (0.116 g, 0.114 mmol) and toluene (10 mL). Cyclopentadiene (0.10 mL, 1.19 mmol) was added to the solution via syringe at 25 °C and the solution was vigorously stirred for 16 h at 25 °C. The color of the solution changed from deep green to dark green. After the volatile materials were removed under reduced pressure, the resulting solid was sensed by 10 mL of acetonitrile two times to remove resulting cyclopentadiene and Cp*CpRu. Dryness in vacuo gave **4** as a purple solid (87.9 mg, 0.105 mmol, 91%). A purple single crystal of **4** was obtained from the cold toluene solution of **4** stored at −30 °C. ^{1}H NMR (400 MHz, THF-d_8, −70 °C): δ −17.27 (s, 3H, μ- or μ$_3$-hydride), −12.92 (s, 3H, μ- or μ$_3$-hydride), 2.04 (s, 45H, C$_5$*Me*$_5$), 5.20 ppm (s, 5H, C$_5$*eH*$_5$). ^{13}C NMR (100 MHz, THF-d_8, 25 °C): δ 13.2 (q, J_{CH} = 126 Hz, C$_5$*Me*$_5$), 89.7 (d, J_{CH} = 173 Hz, *C*$_5$H$_5$), 90.1 ppm (*C*$_5$Me$_5$). Anal. Calcd for C$_{35}$H$_{56}$NiRu$_3$: C, 50.12; H, 6.73. Found: C, 49.92; H, 7.12.

*4.5.5. Reaction of (CpNi)(Cp*Ru)$_3$(μ$_3$-H)$_3$(μ-H)$_3$ (**4**) with 1 atm of D_2*

An NMR tube equipped with a Teflon valve was charged with **4** (5.0 mg, 6.0 μmol) and THF-d_8 (0.4 mL). After the NMR tube was degassed with a liquid N_2 bath, 1 atm of D_2 was introduced. The NMR tube was kept at 25 °C. However, no detectable changes were observed in the ^{1}H NMR spectrum recorded at −60 °C after 72 h.

*4.5.6. Protonolysis of (CpNi)(Cp*Ru)$_3$(μ$_3$-H)$_3$(μ-H)$_3$ (**4**)*

An NMR tube equipped with a Teflon valve was charged with **4** (6.0 mg, 7.2 μmol), CD_2Cl_2 (0.4 mL), and hexamethylbenzene as an internal standard. After an excess amount of HBF_4·Et_2O was added to the solution with a micro syringe (*ca.* 70 equiv), ^{1}H NMR spectrum of the solution was recorded. The ^{1}H NMR spectrum showed the disappearance of **4** accompanied by the exclusive formation of [{Cp*Ru(μ-H)$_2$}$_3$]$^+$ in 83%. [{Cp*Ru(μ-H)$_2$}$_3$]$^+$: ^{1}H NMR (400 MHz, CD_2Cl_2, 25 °C): δ −11.22 (s, 6H, Ru*H*), 1.98 ppm (s, 45H, Cp*).

Acknowledgment

This work was supported by JST CREST, Grant Number JPMJCR15P4.

Appendix A. Supplementary data

Supplementary data to this article can be found online at https://doi.org/10.1016/j.jorganchem.2018.12.016.

References

[1] J.H. Sinfelt, Catalysis by alloys and bimetallic clusters, Acc. Chem. Res. 10 (1977) 15–20.
[2] L. Guczi, Mechanism of reactions on multimetallic catalysts, J. Mol. Catal. 25 (1984) 13–29.
[3] L.J. Farrugia, Heteronuclear clusters containing platinum and the metals of the iron, cobalt, and nickel triads, Adv. Organomet. Chem. 13 (1990) 301–391.
[4] P. Braunstein, J. Rosé, Heterometallic clusters in catalysis, in: P. Braunstein, L.A. Oro, P.R. Raithby (Eds.), Metal Clusters in Chemistry, 2, Wiley-VCH, Weinheim, 1999, pp. 616–617.
[5] P. Buchwalter, J. Rosé, P. Braunstein, Multimetallic catalysis based on heterometallic complexes and clusters, Chem. Rev. 115 (2015) 28–126.
[6] J. Gao, Q. Liu, F. Gu, B. Liu, Z. Zhong, F. Su, Recent advances in methanation catalysts for the production of synthetic natural gas, RSC Adv. 5 (2015) 22759–22776.
[7] T. Minowa, T. Ogi, Hydrogen production from cellulose using a reduced nickel catalyst, Catal. Tody. 45 (1998) 411–416.
[8] M. Marquevich, S. Czernik, E. Chornet, D. Montané, Hydrogen from biomass: steam reforming of model compounds of fast-pyrolysis oil, Energy Fuel. 13 (1999) 1160–1166.
[9] M. Inaba, K. Murata, M. Saito, I. Takahara, Hydrogen production by gasification of cellulose over Ni catalysts supported on zeolites, Energy Fuel. 20 (2006) 432–438.
[10] S.M. Swami, M.A. Abraham, Integrated catalytic process for conversion of biomass to hydrogen, Energy Fuel. 20 (2006) 2616–2622.
[11] T. Furusawa, T. Sato, H. Sugito, Y. Miura, Y. Ishiyama, M. Sato, N. Itoh, N. Suzuki, Hydrogen production from the gasification of lignin with nickel catalysts in supercritical water, Int. J. Hydrogen Energy 32 (2007) 699–704.
[12] P. Azadi, J. Otomo, H. Hatano, Y. Oshima, R. Farnood, Hydrogen production by catalytic near-critical water gasification and steam reforming of glucose, Int. J. Hydrogen Energy 35 (2010) 3406–3414.
[13] Z. Bian, S. Das, M.H. Wai, P. Hongmanorom, S. Kawi, A review on bimetallic nickel-based catalysts for CO_2 reforming of methane, ChemPhysChem 18 (2017) 3117–3134.
[14] D.J. Elliott, J.H. Lunsford, Kinetics of the methanation reaction over Ru, Ru–Ni, Ru–Cu, and Ni clusters in zeolite Y, J. Catal. 57 (1979) 11–26.
[15] A. Chen, T. Miyao, K. Higashiyama, H. Yamashita, M. Watanabe, High catalytic performance of ruthenium-doped mesoporous nickel–aluminum oxides for selective CO methanation, Angew. Chem. Int. Ed. 49 (2010) 9895–9898.
[16] S. Tada, R. Kikuchi, A. Takagaki, T. Sugawara, S.T. Oyama, K. Urasaki, S. Satokawa, Study of Ru Ni/TiO_2 catalysts for selective CO methanation, Appl. Catal. B Environ. 140–141 (2013) 258–264.
[17] S. Tada, R. Kikuchi, K. Wada, K. Osada, K. Akiyama, S. Satokawa, Y. Kawashima, Long-term durability of Ni/TiO_2 and Ru–Ni/TiO_2 catalysts for selective CO methanation, J. Power Sources 264 (2014) 59–66.
[18] S. Li, D. Gong, H. Tang, Z. Ma, Z.-T. Liu, Y. Liu, Preparation of bimetallic Ni@Ru

nanoparticles supported on SiO_2 and their catalytic performance for CO methanation, Chem. Eng. J. 334 (2018) 2167–2178.
[19] C. Crisafulli, S. Scirè, R. Maggiore, S. Miniciò, S. Galvagno, CO_2 reforming of methane over Ni–Ru and Ni–Pd bimetallic catalysts, Catal. Lett. 59 (1999) 21–26.
[20] C. Crisafulli, S. Scirè, S. Minicòs, L. Solarino, Ni–Ru bimetallic catalysts for the CO_2 reforming of methane, Appl. Cat A-Gen. 225 (2002) 1–9.
[21] J.H. Jeong, J.W. Lee, D.J. Seo, Y. Seo, W.L. Yoon, D.K. Lee, D.H. Kim, Ru-doped Ni catalysts effective for the steam reforming of methane without the pre-reduction treatment with H_2, Appl. Catal. A-Gen. 302 (2006) 151–156.
[22] D. Li, I. Atake, T. Shishido, Y. Oumi, T. Sano, K. Takehira, Self-regenerative Activity of Ni/Mg(Al)O catalysts with trace Ru during daily start-up and shut-down operation of CH4 steam reforming, J. Catal. 250 (2007) 299–312.
[23] M. Álvarez, M.Á. Centenom, J.A. Odriozola, Ru–Ni catalyst in the combined dry-steam reforming of methane: the importance in the metal order addition, Top. Catal. 59 (2016) 303–313.
[24] A. Álvarez, L.F. Bobadilla, V. Garcilaso, M.A. Centeno, J.A. Odriozola, CO_2 reforming of methane over Ni–Ru supported catalysts: on the nature of active sites by operando DRIFTS study, J. CO_2 Utl. 24 (2018) 509–515.
[25] X. Chen, N. Yan, Novel catalytic systems to convert chitin and lignin into valuable chemicals, Catal. Surv. Asia 18 (2014) 164–176.
[26] O.U. Valdés-Martínez, V.A. Suárez-Toriello, J.A. de los Reyes, B. Pawelec, J.L.G. Fierro, Support effect and metals interactions for $NiRu/Al_2O_3$, TiO_2 and ZrO_2 catalysts in the hydrodeoxygenation of phenol, Catal. Today 296 (2017), 219–217.
[27] Z. Luo, Z. Zheng, L. Li, Y.-T. Cui, C. Zhao, Bimetallic Ru–Ni catalyzed aqueous-phase guaiacol hydrogenolysis at low H_2 pressures, ACS Catal. 7 (2017) 8304–8313.
[28] Y. Hu, G. Jiang, G. Xu, X. Mu, Hydrogenolysis of lignin model compounds into aromatics with bimetallic Ru–Ni supported onto nitrogen-doped activated carbon catalyst, J. Mol. Catal. 445 (2018) 316–326.
[29] G. Chen, S. Desinan, R. Nechachem R. Rosei, F. Rosei, D. Ma, Bifunctional catalytic/magnetic Ni@Ru core–shell nanoparticles, Chem. Commun. 47 (2011) 6308–6310.
[30] G. Chen, S. Desinan, R. Rosei, F. Rosei, D. Ma, Synthesis of Ni–Ru alloy nanoparticles and their high catalytic activity in dehydrogenation of ammonia borane, Chem. Eur J. 18 (2012) 7925–7930.
[31] N. Cao, J. Su, W. Luo, G. Cheng, Hydrolytic dehydrogenation of ammonia borane and methylamine borane catalyzed by graphene supported Ru@Ni core–shell nanoparticles, J. Hydrogen Energ. 39 (2014) 426–435.
[32] N. Cao, J. Su, X. Hong, W. Luo, G. Cheng, In situ facile synthesis of Ru–Based core–shell nanoparticles supported on carbon black and their high catalytic activity in the dehydrogenation of amine-boranes, Chem. Asian J. 9 (2014) 562–571.
[33] X. Li, C. Zeng, G. Fan, Ultrafast hydrogen generation from the hydrolysis of ammonia borane catalyzed by highly efficient bimetallic RuNi nanoparticles stabilized on $Ti_3C_2X_2$ (X = OH and/or F), Int. J. Hydrogen Energy 40 (2015) 3883–3891.
[34] L.-J. Lim, W.-J. Yi, T.-W. Liu, C. Huang, Z.-S. Chao, Hydrogenation of 3-hydroxypropanal into 1,3-propanediol over bimetallic Ru–Ni catalyst, RSC Adv. 7 (2017) 32027–32037.
[35] G. Predieri, P. Moggi, S. Papadopulos, A. Armigliato, S. Bigi, E. Sappa, Characterization of an ultrafine Ni–Ru alloy powder and of alumina-dispersed bimetallic particles derived from the molecular cluster $(C_5H_5)NiRu_3H_3(CO)_9$, J. Chem. Soc., Chem. Commun. (1990) 1736–1737.
[36] A. Armigliato, S. Bigi, P. Moggi, S. Papadopulos, G. Predieri, G. Salviati, E. Sappa, Production of Ni–Ru bimetallic catalysts and materials by thermal and chemical decomposition of a tetranuclear bimetallic carbonyl cluster, Mater. Chem. Phys. 29 (1991) 251–260.
[37] J.M. Rynkowski, T. Paryjczak, M. Lenik, Characterization of alumina supported Nickel–Ruthenium systems, Appl. Catal. A-Gen. 126 (1995) 257–271.
[38] M. Cerro-Alarcón, A. Maroto-Valiente, I. Rodríguez-Ramos, A. Guerrero-Ruiz, Surface study of graphite-supported Ru–Co and Ru–Ni bimetallic catalysts, Appl. Catal. A-Gen. 275 (2004) 257–269.
[39] P. Braos-García, C. García-Sancho, A. Infantes-Molina, E. Rodríguez-Gastellón, A. Jiménez-López, Bimetallic Ru/Ni supported catalysts for the gas phase hydrogenation of acetonitrile, Appl. Catal. A-Gen. 381 (2010) 132–144.
[40] F. Lange, U. Armbruster, A. Martin, Heterogeneously-catalyzed hydrogenation of carbon dioxide to methane using RuNi bimetallic catalysts, Energy Technol. 3 (2015) 55–62.
[41] M.Z. Hossain, M.B.I. Chowdhury, A.K. Jhawar, P.A. Charpentier, Supercritical water gasification of glucose using bimetallic aerogel $Ru–Ni–Al_2O_3$ catalyst for H_2 production, Biomass Bioenergy 107 (2017) 39–51.
[42] K.C. Pingali, S. Deng, D.A. Rockstraw, Direct Synthesis of Ru–Ni Core-and-shell Nanoparticles by Spray-pyrolysis: Effects of Temperature and Precursor Constituent Ratio, 183, 2008, pp. 282–289.
[43] K.C. Pingali, S. Deng, D.A. Rockstraw, Synthesis and thermal stability of carbon-supported Ru–Ni core-and-shell nanoparticles, Powder Technol. 187 (2008) 19–26.
[44] E. Sappa, A. Tiripicchio, M.T. Camellini, A new, mixed ruthenium-nickel cluster. Synthesis and X-ray crystal structure of $(\eta^5\text{-}C_5H_5)\ NiRu_3(CO)_9C{\cdot}C(H)\ bu^t$, J. Chem. Soc., Chem. Commun. (1979) 254. This complex was originally characterized as (η5-C5H5)NiRu3(μ4-η2-C=CtBuH)(CO)9, however the structure was revised as (η5-C5H5)NiRu3(μ-H)(μ4-η2-C=CtBuH)(CO)9 later in ref [45].
[45] E. Sappa, A.M.M. Lanfredi, A. Tiripicchio, The reactions of ruthenium carbonyl and alkyne-carbonyl complexes with nickelocene, $[(\eta\text{-}C_5H_5)Ni(CO)]_2$ and $(\eta\text{-}C_5H_5)_2Ni_2(RC_2R')$. Crystal structures of two isostructural heterometallic trinuclear clusters, $(\eta\text{-}C_5H_5)_2Ni_2Ru(CO)_3(C_2Ph_2)$ and $(\eta\text{-}C_5H_5)_2Ni_2Fe(\text{-}CO)_3(C_2Ph_2)$, J. Organomet. Chem. 221 (1981) 93–110.
[46] A. Tiripicchio, M.T. Camellini, E. Sappa, The influence of molecular hydrogen on the reaction between $[Ru_3(CO)_{12}]$ and $[Ni_2(\eta\text{-}C_5H_5)(C_2Ph_2)]$. Synthesis and crystal structure of the new heteropentametallic cluster $[Ni_2Ru_3(\eta\text{-}C_5H_5)_2(CO)_6(\mu\text{-}CO)_2(\mu_4,\eta^2\text{-}C_2Ph_2)]$, J. Chem. Soc., Dalton Trans. (1984) 627–632.
[47] E. Sappa, A. Tiripicchio, M.T. Camellini, Synthesis and crystal structure of $(\eta^5\text{-}C_5H_5)_2Ru_2Ni(CO)_3(\mu_3\text{-}CO)(C_2Ph_2)$. Facile, one step synthesis of a chiral complex, J. Organomet. Chem. 213 (1981) 175–184.
[48] E. Sappa, A. Tiripicchio, M.T. Camellini, The reactivity of $HRu(CO)_9C_2Bu^t$. Synthesis and crystal structure of $(\eta^5\text{-}C_5H_5)NiRu_3(CO)_9C{\cdot}C(H)bu^t$, a new mixed Ruthenium–Nickel cluster, Inorg. Chim. Acta. 41 (1980) 11–17.
[49] D. Osella, E. Sappa, A. Tiripicchio, M.T. Camellini, Synthesis and structural characterization of the isomeric Ruthenium–Nickel derivatives $(\eta\text{-}C_5H_5)NiRu_3(CO)_8(C_6H_9)$ and related complexes, Inorg. Chim. Acta. 42 (1980) 183–190.
[50] A.J. Carty, N.J. Taylor, E. Sappa, A. Tiripicchio, Multisite-bound vinylidenes on heterometallic clusters. Reformulation of $(\eta^5\text{-}C_5H_5Ni)Ru_3(CO)_9(\mu_4\text{-}\eta^2\text{-}C{=}CHR)$ (R = *t*-bu) as hydrido-bridged $(\mu\text{-}H)(\eta^5\text{-}C_5H_5Ni)Ru_3(CO)_9(\mu_4\text{-}\eta^2\text{-}C{=}CHR)$. Molecular structure of the isopropyl derivative (R = *i*-Pr) and an improved synthetic method, Inorg. Chem. 22 (1983) 1871–1876.
[51] G. Lavigne, F. Papageorgiou, C. Bergounhou, J.-J. Bonnet, Synthesis and spectroscopic characterization of trihydrido mixed-metal tetranuclear clusters $(\mu\text{-}H)_3M_3Ni(\eta^5\text{-}C_5H_5)(CO)_9$ (M = Ru, Os). Low-temperature X-ray diffraction study of the osmium derivative, Inorg. Chem. 22 (1983) 2485–2491.
[52] M. Castiglioni, R. Giordano, E. Sappa, Phosphine-substituted and phosphido-bridged metal clusters in homogeneous catalysis I. Synthesis and reactivity of $(\eta^5\text{-}C_5H_5)NiM_3(\mu\text{-}H)_3(CO)_{9-n}L_n$, M = Ru, Os, *n* = 1, 2: L = PPh_3, PPh_2H, PCy_3, PEt_3) and $M_3(CO)_{12-n}L_n$ (M = Ru, *n* = 1–3: L = PPh_3, PPh_2H, PCy_3, PEt_3; M = Os, *n* = 1, 2: L = PPh_3), J. Organomet. Chem. 342 (1988) 97–109.
[53] E. Brivio, A. Ceriotto, R.D. Pergola, L. Garlaschelli, M. Manassero, M. Sansoni, Nickel–Ruthenium mixed-metal carbonyl clusters. Syntheses and solid state structures of the two tetrahedral clusters $[PPh_4][NiRu_3(\mu_3\text{-}H)(CO)_9(\mu\text{-}CO)_3]$ and $[NEt_4]_2[NiRu_3(CO)_8(\mu\text{-}CO)_4]$, J. Cluster Sci. 6 (1995) 271–287.
[54] M. Lanfranchi, A. Tripicchio, M.T. Camellini, O. Gambino, E. Sappa, Synthesis and crystal structure of $(\eta\text{-}C_5H_5)_2Ni_2Ru_2(CO)_6[C_2(H)C(=CH_2)CH_3]$. A new heterometallic cluster with an uncommon metal atom framework, Inorg. Chim. Acta. 64 (1982) L269–L271.
[55] M. Lanfranchi, A. Tiripiccio, E. Sappa, S.A. MacLaughlin, A.J. Carty, $NiRu_4(CO)_9(\mu\text{-}PPh_2)_2(\mu_4\text{-}C{\equiv}CPr^i)_2$: a pentanuclear mixed metal cluster with a novel metal framework, J. Chem. Soc., Chem. Commun. (1982) 538–539.
[56] P. Blenkiron, G.D. Enright, A.J. Carty, Polycarbon ligand chemistry. Novel behaviour of $\mu\text{-}\eta^1,\eta^2_{\alpha,\beta}$-Butadiynyls towards metal fragment additions, Chem. Commun. (1997) 483–484.
[57] M.J. Biatek, L. Latos-Grażyński, Merging of inner and outer ruthenium organometallic coordination motifs within an azuliporphyrin framework, Chem. Commun. 50 (2014) 9270–9272.
[58] M. Lanfranchi, A. Tiripicchio, E. Sappa, A.J. Carty, Crystal structure of $[Ni_2Ru_3(\eta\text{-}C_5H_5)_2(CO)_9(\mu_5\text{-}PPh)]$, an open square-pyramidal cluster obtained via condensation of coordinatively unsaturated $[Ru_3(\mu\text{-}H)(CO)_9(\mu\text{-}PPh_2)]$ with $[Ni_2(\eta\text{-}C_5H_5)_2(CO)_2]$, J. Chem. Soc., Dalton Trans. (1986) 2737–2740.
[59] T. Khimyak, B.F.G. Johnson, High-yield synthesis of new Ni–Ru carbido–carbonyl clusters, J. Cluster Sci. 15 (2004) 543–558.
[60] S. Saha, L. Zhu, B. Captain, Bimetallic octahedral Ruthenium–Nickel carbido cluster complexes. Synthesis and structural characterization, Inorg. Chem. 52 (2013) 2526–2532.
[61] M.P. Jensen, W. Henderson, D.H. Johnston, M. Sabat, D.F. Shriver, The ketenylidene route to mixed-metal carbide clusters: $[MnRu_3C(CO)_{13}]^-$, $[MnOs_3C(CO)_{13}]^-$, $[Cr_2Ru_3C(CO)_{16}]^{2-}$, $[Mo_2Ru_3C(CO)_{16}]^{2-}$, $[Rh_3Ru_3C(CO)_{15}]^-$, $[Ni_3Ru_3C(CO)_{13}]^{2-}$ and $[Co_3Ru_3C(CO)_{15}]^-$, J. Organomet. Chem. 394 (1990) 121–143.
[62] M. Plois, W. Hujo, S. Grimme, C. Schwickert, E. Bill, B. de Bruin, R. Pöttgen, R. Wolf, Open-shell first-row transition-metal polyhydride complexes based on the *fac*-$[RuH_3(PR3)_3]^-$ bbuilding block, Angew. Chem. Int. Ed. 52 (2013) 1314–1318.
[63] S. Ogo, R. Kabe, K. Uehara, B. Kure, T. Nishimura, S.C. Menon, R. Harada, S. Fukuzumi, Y. Higuchi, T. Ohhara, T. Tamada, R. Kuroki, A dinuclear Ni(μ-H) Ru complex derived from H_2, Science 316 (2007) 585–586.
[64] G.M. Chambers, R. Angamuthu, D.L. Gray, T.B. Rauchfuss, Organo Ruthenium–Nickel dithiolates with redox-responsive nickel sites, Organometallics 32 (2013) 6324–6329.
[65] T. Kuzutani, Y. Torihata, H. Suzuki, T. Takao, Synthesis of a heterometallic trinuclear cluster of ruthenium and platinum with a linear alignment, Organometallics 35 (2016) 2543–2556.
[66] T. Nakajima, I. Shimizu, K. Kobayashi, Y. Wakatsuki, Synthesis of triangular and tetrahedral heteronuclear metal clusters using hydride complexes of cyclopentadienylrhodium and -ruthenium as the precursors, Organometallics 7 (1998) 262–269.
[67] H. Suzuki, T. Kakigano, K. Tada, M. Igarashi, K. Matsubara, A. Inagaki, M. Oshima, T. Takao, Synthesis, structures, and reactions of coordinatively unsaturated trinuclear ruthenium polyhydrido complexes, $[\{Ru(C_5Me_5)\}_3(\mu\text{-}H)_6](Y)$ (Y = BF_4, CF_3SO_3, 1/2(SO_4), $C_6H_5CO_2$, CH_3CO_2, $B(C_6H_5)_4$, PF_6) and

[{Ru(C_5Me_5)}$_3$(μ-H)$_3$(μ_3-H)$_2$], Bull. Chem. Soc. Jpn. 78 (2005) 67–87.
[68] H. Kameo, Y. Ito, R. Shimogawa, A. Koizumi, H. Chikamori, J. Fujimoto, H. Suzuki, T. Takao, Synthesis and characterisation of tetranuclear ruthenium polyhydrido clusters with pseudo-tetrahedral geometry, Dalton Trans. 46 (2017) 5631–5643.
[69] R.D. Adams, Q. Zhang, Structures and bonding of η^2-bridging CO ligands and their influence on the structures and rearrangements of higher nuclearity metal carbonyl cluster complexes, Organometallics 32 (2013) 5171–5179.
[70] R.A.A.-M. Muna, J. Lewis, P.R. Raithby, A novel arene bonding mode in the mixed-metal cluster $Os_4Ru(\mu\text{-}H)_3(CO)_{12}(\mu\text{-}\eta^6\text{-}C_6H_6)P(OMe)_3$, J. Organomet. Chem. 530 (1997) 247–250.
[71] J.W.-S. Hui, W.-T. Wong, Reaction of $[Os_3(\mu\text{-}H)_2(CO)_{10}]$ with *trans*-$[Pd(NH_3)_2I_2]$; molecular structures of $[Os_6Pd(\mu\text{-}H)_8(CO)_{18}]$, $[Os_4Pd(\mu\text{-}H)_4(CO)_{12}(\mu\text{-}I)_2]$, $[Os_4Pd(\mu\text{-}H)_3(CO)_{12}(\mu\text{-}I)_3]$ and $[\{Os_3Pd(\mu\text{-}H)_3(CO)_9(\mu\text{-}I)\}_2]$, J. Chem. Soc., Dalton Trans. (1997) 1515–1520.
[72] J.P.-K. Lau, W.-T. Wong, Synthesis, structural characterization and solution dynamics of osmium–rhodium mixed-metal cluster $[Os_4Rh(\mu\text{-}H)_4(CO)_{13}(\eta^2\text{-}NC_5H_4C_2H_2)]$, Inorg. Chem. Commun. 6 (2003) 174–177.
[73] J.P. Canal, G.P.A. Yap, R.K. Pomeroy, The $ReOs_4(\mu\text{-}H)(CO)_n$ (n = 19, 18, 16) Clusters, Organometallics 22 (2003) 3439–3447.
[74] K. Uehara, S. Hikichi, M. Akita, Reactivity control of a dinuclear xenophilic species, $Tp^{\#}Ni–RuCp(CO)_2$, via spin crossover across a metal-metal bond [$Tp^{\#}$: hydrotris(4-bromo-3,5-dimethylpyrazolyl)borato], Chem. Lett. (2002) 1198–1199.
[75] F. Carniato, G. Gatti, G. Gervasio, D. Marabello, E. Sappa, A. Secco, Synthesis and structure of new phosphine-substituted Homo- and hetero-bimetallic carbonyl clusters of iron, ruthenium and nickel. Characterization of two inorganic–organometallic hybrid materials based on mesoporous SBA-15 silica, Inorg. Chim. Acta. 363 (2010) 1773–1778.
[76] T. Takao, N. Obayashi, B. Zho, K. Akiyoshi, H. Omori, H. Suzuki, Synthesis and property of diruthenium complexes containing bridging cyclic diene ligands and the reaction of diruthenium tetrahydrido complex with benzene forming a μ-η^2:η^2-Cyclohexadiene complex via partial hydrogenation on a Ru_2 center, Organometallics 30 (2011) 5057–5067.
[77] M. Castiglioni, R. Giordano, E. Sappa, Homogenous catalytic hydrogenation and isomerization of linear and cyclic monoenes and dienes in the presence of the heterometallic cluster $(\eta^5\text{-}C_5H_5)NiRu_3(\mu\text{-}H)_3(CO)_9$, J. Organomet. Chem. 319 (1987) 167–181.
[78] H. Suzuki, H. Omori, D.H. Lee, Y. Yoshida, M. Fukushima, M. Tanaka, Y. Moro-oka, Synthesis, structure, and chemistry of a dinuclear tetrahydride-bridged complex of ruthenium, $(\eta^5\text{-}C_5Me_5)Ru(\mu\text{-}H)_4Ru(\eta^5\text{-}C_5Me_5)$. C–H bond activation and coupling reaction of ethylene on dinuclear complexes, Organometallics 13 (1994) 1129–1146.
[79] PROCESS-AUTO, Automatic Data Acquisition and Processing Package for Imaging Plate Diffractometer, Rigaku Corporation, Tokyo, Japan, 2015.
[80] G.M. Sheldrick, SHELXT - integrated space-group and crystal-structure determination, Acta Crystallogr. A: Found. Crystallogr. A71 (2015) 3–8.
[81] G.M. Sheldrick, Crystal structure refinement with SHELXL, Acta Crystallogr. C: Struct. Chem. C71 (2015) 3–8.
[82] A. Thorn, B. Dittrich, G.M. Sheldrick, Enhanced rigid-bond restraints, Acta Crystallogr. A: Found. Adv. A68 (2012) 448–451.
[83] D. Andrae, U. Häußermann, M. Dolg, H. Stoll, H. Preuß, Energy-adjustedab initio pseudopotentials for the second and third row transition elements theor, Chim. Acta 77 (1990) 123–141.
[84] J.D. Chai, M. Head-Gordon, Long-range corrected hybrid density functionals with damped atom-atom dispersion corrections, Phys. Chem. Chem. Phys. 10 (2008) 6615–6620.
[85] Gaussian 16, Revision A.03, M.J. Frisch, G.W. Trucks, H.B. Schlegel, G.E. Scuseria, M.A. Robb, J.R. Cheeseman, G. Scalmani, V. Barone, G.A. Petersson, H. Nakatsuji, X. Li, M. Caricato, A.V. Marenich, J. Bloino, B.G. Janesko, R. Gomperts, B. Mennucci, H.P. Hratchian, J.V. Ortiz, B. Izmaylov, A.F. Sonnenberg, J.L. Williams-Young, D. Ding, F. Lipparini, F. Egidi, F. Goings, J. Peng, A. Petrone, T. Henderson, D. Ranasinghe, V.G. Zakrzewski, J. Gao, N. Rega, G. Zheng, W. Liang, M. Hada, M. Ehara, K. Toyota, R. Fukuda, J. Hasegawa, M. Ishida, T. Nakajima, Y. Honda, O. Kitao, H. Nakai, T. Vreven, K. Throssell, J.A. Montgomery Jr., J.E. Peralta, F. Ogliaro, M.J. Bearpark, J.J. Heyd, E.N. Brothers, K.N. Kudin, V.N. Staroverov, T.A. Keith, R. Kobayashi, J. Normand, K. Raghavachari, A.P. Rendell, J.C. Burant, S.S. Iyengar, J. Tomasi, M. Cossi, J.M. Millam, M. Klene, C. Adamo, R. Cammi, J.W. Ochterski, R.L. Martin, K. Morokuma, O. Farkas, J.B. Foresman, D.J. Fox, Gaussian, Inc., Wallingford CT, 2016.
[86] R.D. Dennington II, T.A. Keith, J. Millam, Semichem Inc., Shaw-nee Mission KS, 2016.